

Time domain inverse scattering for a buried homogeneous cylinder in a slab medium using NU-SSGA

Chien-Ching Chiu^{a,*} and Chung-Hsin Huang^b

^a*Electrical Engineering Department, Tamkang University, New Taipei City, Taiwan, China*

^b*Department of Computer and Communication Engineering, Taipei College of Maritime Technology, New Taipei City, Taiwan, China*

Abstract. A time-domain inverse scattering technique for reconstructing a buried homogeneous cylinder with arbitrary cross section in a slab medium is proposed. For the forward scattering, the FDTD method is employed to calculate the scattered E fields. Base on the scattering fields, these inverse scattering problems are transformed into optimization problems. The non-uniform steady state genetic algorithm (NU-SSGA) is applied to reconstruct the location shape and permittivity of the two-dimensional homogeneous dielectric cylinder. The NU-SSGA is a population-based optimization approach that aims to minimize the objective function between measurements and computer-simulated data. A set of representative numerical results is presented for demonstrating that the proposed approach is able to efficiently reconstruct the electromagnetic properties of homogeneous dielectric scatterer even when the initial guess is far away from the exact one. In addition, the effects of Gaussian noises on the image reconstruction are also investigated.

Keywords: Time domain inverse scattering, microwave imaging, FDTD, subgridding FDTD, NU-SSGA

1. Introduction

The problem of reconstructing two/three-dimensional objects buried in layered media is an important research issue [1–10]. It is useful in geophysical exploration, target identification, environmental survey, microwave imaging and nondestructive testing. However, it is well known that one major difficulty of inverse scattering is its ill-posedness in nature [11]. In general, the ill-posed problem can be treated by regularization schemes or transformed into a better conditioned problem [12]. Moreover, the fact that the inverse problem is nonlinear is due to the dependence of scattering fields upon the electromagnetic properties of scatterer and total field in the scatterer domain simultaneously. The nonlinearity of the problem is treated and resolved by using iterative optimization techniques.

Previously, many methods have been applied to solve inverse problem, such as genetic algorithm (GA) [13–15], Born iteration method (BIM) [16], particle swarm optimization (PSO) [17], distorted Born iteration method (DBIM) [18] and Newton-Kantorovitch algorithm [19–21]. Recent research [22] has shown that the NU-SSGA outperforms a simple genetic algorithm (SGA) on large set of optimization

*Corresponding author: Chien-Ching Chiu, Electrical Engineering Department, Tamkang University, New Taipei City, Taiwan, China. E-mail: chiu@ee.tku.edu.tw.

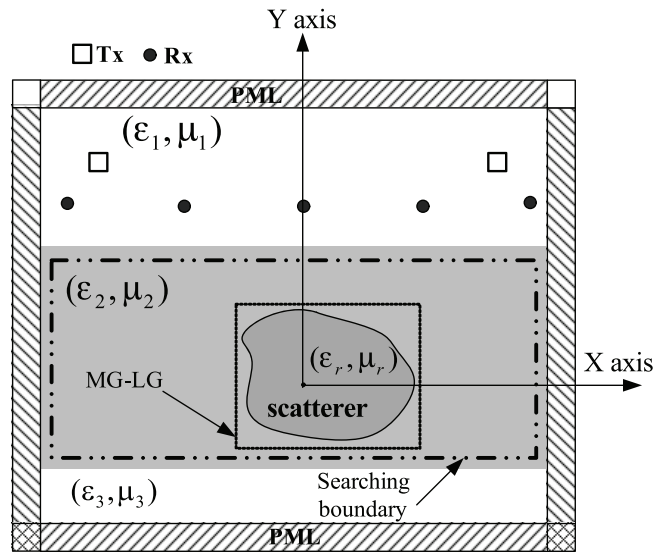


Fig. 1. Geometrical configuration for the inverse scattering.

problems in terms of both speed and accuracy in some cases. However, these papers are focused on frequency-domain.

Time domain inverse scattering problems appear quite a lot in the area of remote sensing. As compared to frequency-domain approach, the interaction of the entire medium in the time domain with the incident field needs to be considered. In contrast, time-domain approaches can exploit causality to limit the region of inversion, potentially reducing the number of unknowns. In past years, fewer researchers had applied the GA in the time domain inverse scattering problem for the metallic target identification [23] and dielectric object reconstruction [24–26]. To the best of our knowledge, there is still no investigation on using the GA to reconstruct the location, shape function and permittivity of 2D homogeneous dielectric cylinders imaging problem in a slab medium under time domain.

In this paper, the forward problem is solved based on the FDTD method, for which the sub-gridding technique is implemented to closely describe the fine structure of the cylinder [27]. Interpolation technique through the closed cubic B-splines [28] is employed to describe a cylinder with arbitrary shape more effectively instead of the frequently used trigonometric series expansion. The inverse problem is formulated into an optimization one and then the non-uniform steady state genetic algorithm (NU-SSGA) [22] previously published by the authors is used to search the parameter space.

In session II, the subgridding FDTD methods for the forward scattering are presented. In session III, the numerical results of the proposed inverse problem are given. Finally, in session IV some conclusions are drawn for the proposed time domain inverse scattering.

2. Forward problem

Consider a 2-D homogeneous dielectric cylinder buried in a slab medium material medium as shown in Fig. 1. The cylinder is parallel to z axis buried below a planar interface separating three homogeneous spaces: the air (ϵ_1, μ_1) , the earth (ϵ_2, μ_2) and air (ϵ_3, μ_3) . The cross section of the object is star-like shape that can be represented in polar coordinates in the x - y plane with respect to the center position (X_O, Y_O) .

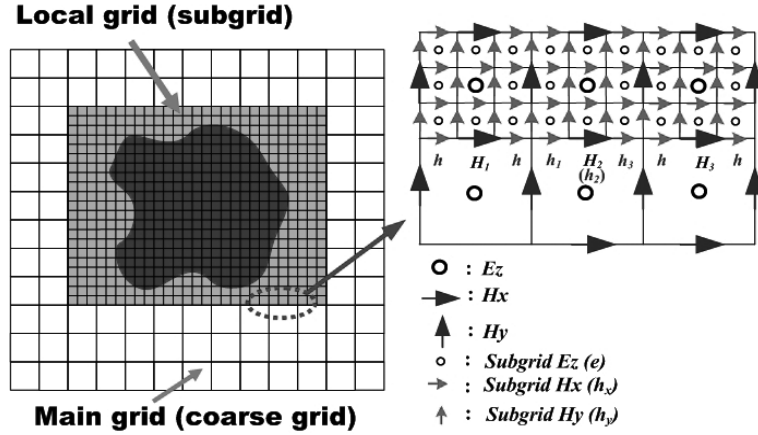


Fig. 2. The structure of the TM_z FDTD major grids and local grids for the scaling ratio (1:3) : H fields are aligned with the MG-LG boundary.

The permittivity and permeability of the buried dielectric object are denoted by (ϵ_r, μ_r) , respectively. The computational domain is discretized by using Yee cells [29]. It should be mentioned that the computational domain is surrounded by optimized absorber of the perfect matching layer (PML) [30] to reduce the reflection from the environment PML interface.

2.1. Forward problem

The direct scattering problem is to calculate the scattered electric fields while the shape, location and permittivity of the scatterer is given. The shape function $F(\theta)$ of the scatterer is described by the trigonometric series in the direct scattering problem

$$F(\theta) = \sum_{n=0}^{N/2} B_n \cos(n\theta) + \sum_{n=1}^{N/2} C_n \sin(n\theta) \quad (1)$$

In order to closely describe the shape of the cylinder for both the forward and inverse scattering procedure, the subgridding technique is implemented in the FDTD code, the details are presented next.

2.2. Subgrid FDTD

A major problem in EM modeling by FDTD method is local fine structures. These structures require a finer cell size than elsewhere and overload the computation cost. The subgridding scheme is proposed to overcome the above drawback in FDTD. A subgridding scheme is employed to divide the problem space into regions with different grid sizes. The grid size in coarse region is about $(\frac{1}{20} \sim \frac{1}{10} \lambda_{\max})$ as in normal FDTD, while in the fine region the grid size is scaled by an integer ratio. As an example, the Yee cells with subgridding structure are shown in Fig. 2, of which the scaling ratio is 1:3. The capital and small case letters stand for EM fields on the major grids and local grids, respectively. If the scaling ratio is set at odd-ratio then the fields are collocated in space at coarse and fine region. The e and fields inside the fine region can be updated through the normal Yee-cell algorithm except those at the MG-LG boundary. The noncollocated magnetic field at the MG-LG interface can be obtained by linearly interpolation. The time interpolation of the fine grid magnetic field at the MG-LG interface is performed using the parabolic

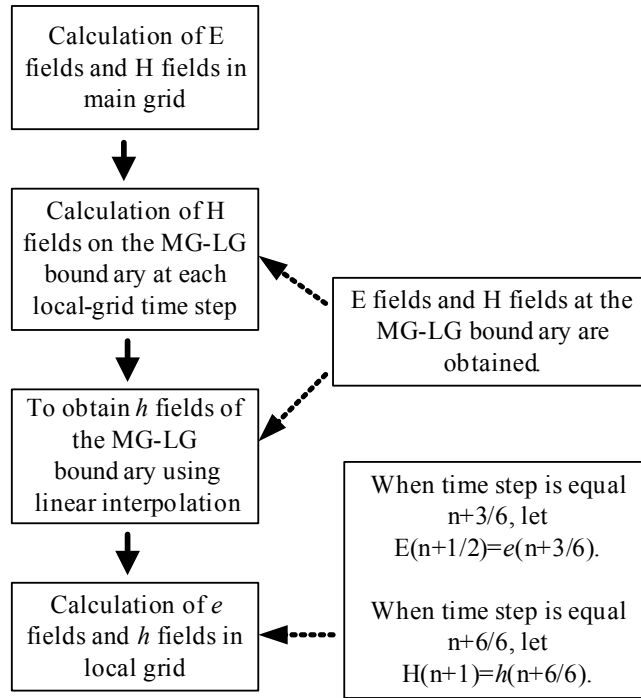


Fig. 3. Flowchart to update the (E,H) fields on the major grids and (e, h) fields on local grids.

interpolation calculation. The above is only a brief introduction to the subgridding FDTD. More detail on subgridding FDTD can be found in [27]. The flow chart associated upon subgrid FDTD computing procedure is shown in Fig. 3.

For the time domain scattering and/or inverse scattering problem, the scatterers can be assigned with the fine region such that the fine structure can be easily described. If higher resolution is needed, only the fine region needs to be rescaled using a higher ratio for subgridding. This can avoid gridding the whole problem space using the finest resolution such that the computational resources are utilized in a more efficient way, which is quite important for the computational intensive inverse scattering problems.

3. Inverse problem

3.1. Inverse problem

For the inverse scattering problem, the shape, location and permittivity of the dielectric cylinder are reconstructed by the given scattered electric field obtained at the receivers. This problem is resolved by an optimization approach, for which the global searching scheme UN-SSGA is employed to minimize the following objective function (OF):

$$OF = \frac{\sum_{n=1}^{N_i} \sum_{m=1}^M \sum_{s=0}^S |E_z^{exp}(n, m, s\Delta t) - E_z^{cal}(n, m, s\Delta t)|}{\sum_{n=1}^{N_i} \sum_{m=1}^M \sum_{t=0}^T |E_z^{exp}(n, m, s\Delta t)|} \quad (2)$$

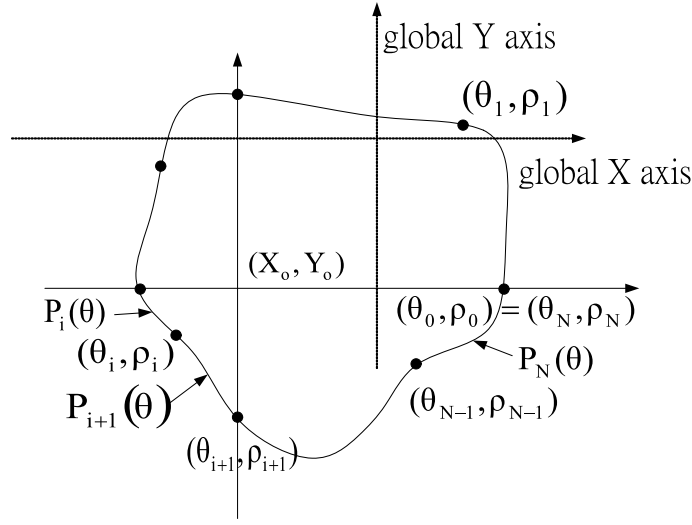


Fig. 4. Geometry of the cubic-spline. (θ_i, ρ_i) is the polarized-coordinate expression for each point and $P_i(\theta)$ is the function of the cubic line which links the points $(\theta_{i-1}, \rho_{i-1})$ and (θ_i, ρ_i) .

where E_z^{exp} and E_z^{cal} are experimental electric fields and the calculated electric fields, respectively. The N_i and M are the total number of the transmitters and receivers, respectively. S is the total time step number of the recorded electric fields.

3.2. Cubic spline interpolation technique

In order to reduce the unknowns required to describe a cylinder of arbitrary cross section, the shape function of the cylinder is expressed in terms of a cubic spline. As shown in Fig. 4, the cubic spline consists of the polynomials of degree 3 $P_i(\theta)$, $i = 1, 2, \dots, N$, which satisfy the following smooth conditions:

$$\begin{aligned}
 P_i(\theta_i) &= P_{i+1}(\theta_i) \equiv \rho_i \\
 P'_i(\theta_i) &= P'_{i+1}(\theta_i) \quad i = 1, 2, \dots, N \\
 P''_i(\theta_i) &= P''_{i+1}(\theta_i)
 \end{aligned} \tag{3}$$

and

$$\begin{aligned}
 P_1(\theta_0) &= P_N(\theta_N) \\
 P'_1(\theta_0) &= P'_N(\theta_N) \equiv \rho'_N \\
 P''_N(\theta_i) &= P''_N(\theta_N)
 \end{aligned} \tag{4}$$

Through the interpolation of the cubic spline, an arbitrary smooth cylinder can be easily described through the radius parameters $\rho_1, \rho_2, \dots, \rho_N$ and the slope ρ'_N , of which the details are referred to [28]. By combining the NU-SSGA and the cubic spline interpolation technique, we are able to reconstruct the microwave image efficiently.

3.3. Non-uniform steady-state genetic algorithm (NU-SSGA)

The non-uniform steady-state genetic algorithm (NU-SSGA) was developed and first applied into inverse scattering problem by Chien-Ching Chiu in [22]. The NU-SSGA is very powerful stochastic global optimization methods based on genetic recombination and evaluation in nature. In general, the NU-SSGA must be able to perform seven basic tasks:

1. Encode the solution parameters as genes.
2. Create a string of the genes to form a chromosome.
3. Initialize a starting population.
4. Evaluate and assign fitness values to individuals in the population.
5. Perform reproduction through some selection scheme.
6. Perform recombination of genes to produce offspring.
7. Perform mutation of genes to produce offspring.

The key distinction between an NU-SSGA and a typical GAs is in the number of fitness calculation. In a typical GAs, each generation of the algorithm replaces the population with the new population. On the contrary, NU-SSGA only needs to generate a few offspring, by non-uniform beta distribution in crossover and mutation, to replace the weakest individual in each new generation. The non-uniform probability density scheme in genetic operator could increase the searching diversity in the early iteration, and also increase the exploration ability of the algorithm in latter iteration. In other words, the number of fitness calculation corresponding to the new population is large in a typical GA compared with NU-SSGA. To prevent the superior individual from been lost during the GA optimization process, the rank scheme is employed in the selection operation for which copies the superior individual to the next generation. Based on the characteristic of NU-SSGA in reducing the numbers of fitness calculation, we are able to reconstruct the microwave image efficiently. The details see [31]. It should be noted that the dielectric constant and center position of the cylinder plus the radii of the geometrical spline used to describe the shape of the cylinder will be determined by the NU-SSGA optimization scheme.

4. Numerical results

As shown in Fig. 1, the problem space is divided in grids with the grid size $\Delta x = \Delta y = 5.95$ mm. The metallic cylinder is buried in lossless slab medium ($\sigma_1 = \sigma_2 = \sigma_3 = 0$). The transmitters and receivers are placed in free space above the homogeneous dielectric. The permittivities in region 1, region 2 and region 3 are characterized by $\varepsilon_1 = \varepsilon_0$, $\varepsilon_2 = 8\varepsilon_0$ and $\varepsilon_3 = \varepsilon_0$, respectively, while the permeability μ_0 is used for each region, i.e., only nonmagnetic media are concerned here.

The scatterer is illuminated by cylindrical waves with the electric field polarized along the axis, while the time dependence of the field is of a one derivative Gaussian pulse. The cylindrical object is illuminated by a transmitter at two different positions, $N_i = 2$, which are located at the $(-143$ mm, 178.5 mm) and $(143$ mm, 178.5 mm), respectively. The scattered E fields for each illumination are collected at the five receivers, $M = 5$, which are equally separated by 47.8 mm along the distance of 48 mm from the interface between region 1 and region 2.

Note that in order to describe the shape of the cylinder more accurately, the subgridding FDTD technique is employed both in the forward scattering (1:9) and the inverse scattering (1:5) parts – but with different scaling ratios as indicated in the parentheses. For the forward scattering, the E fields generated by the FDTD with finer subgrids are used to mimic the experimental data in Eq. (2).

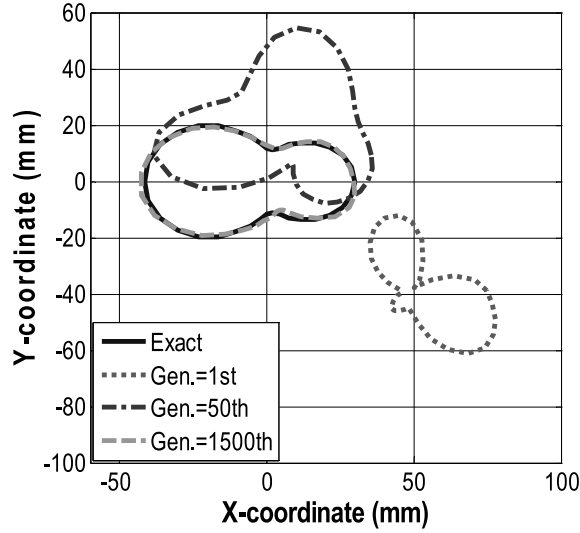


Fig. 5. The reconstructed shape of the cylinder at different generations for example 1.

Two examples are investigated for the inverse scattering of the proposed structure by using NU-SSGA. There are twelve unknown parameters to retrieve, which include the center position (X_O, Y_O) , the radius $\rho_i, i = 1, 2, \dots, 8$ of the shape function and the slope ρ'_N plus the relative permittivity of the object. Very wide searching ranges are used for the NU-SSGA to optimize the objective function given by Eq. (2). The parameters and the corresponding searching ranges are listed follow: $-208.3 \text{ mm} \leq X_O \leq 208.3 \text{ mm}$, $-137.8 \text{ mm} \leq Y_O \leq 77.4 \text{ mm}$, $5.95 \text{ mm} \leq \rho_i \leq 71.4 \text{ mm}, i = 1, 2, \dots, 8$, $-1 \leq \rho'_N \leq 1$ and $1 \leq \varepsilon_r \leq 16$. The relative coefficients of the NU-SSGA are set as below: The crossover rate and the mutation rate are set to 0.1 and 0.05, respectively. The population size set 144 and the rank is set to 108. The typical CPU time for each example is about 20 hours on a home-made Fortran program that runs on an Intel PC (3.4 GHz/4 G memory/500 G).

The first example, a simple cylinder is tested, of which the shape function $F(\theta)$ is chosen to be $F(\theta) = 23.8 - 5.95 \cos(\theta) + 11.9 \cos(2\theta)$ mm, and the relative permittivity of the object is $\varepsilon_r = 3.7$. The reconstructed shape function of the best individual is plotted in Fig. 5 for different generation. The r.m.s. error (DF) of the reconstructed shape $F^{cal}(\theta)$ and the relative error ($DIPE$) of ε_r^{cal} with respect to the exact values versus generation are shown in Fig. 6.

$$DF = \left\{ \frac{1}{N'} \sum_{i=1}^{N'} [F^{cal}(\theta_i) - F(\theta_i)]^2 / F^2(\theta_i) \right\}^{1/2} \quad (5)$$

$$DIPE = \frac{|\varepsilon_r^{cal} - \varepsilon_r|}{\varepsilon_r} \quad (6)$$

where the N' is set to 720. The r.m.s. error DF is about 6.1% and $DIPE = 0.03\%$ in final. It is seen that the reconstruction is good.

The reconstructed images for different generations and the relative error of the second example are shown in Figs 7 and 8, respectively. The shape function of this object is given by $F(\theta) = 23.8 + 5.95 \cos(4\theta) + 17.85 \sin(\theta)$ mm and the relative permittivity of the object is $\varepsilon_r = 5.5$. Figure 8 shows

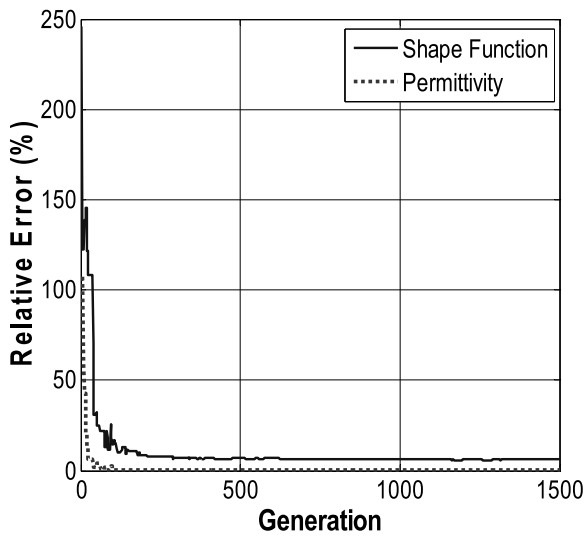


Fig. 6. Shape function error and permittivity error at each generation of example 1.

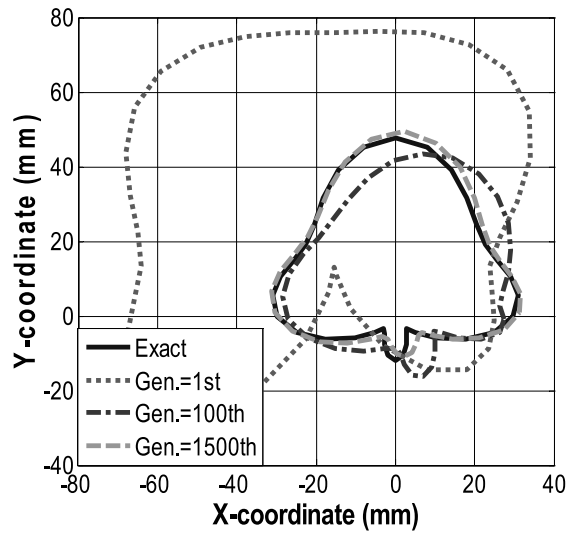


Fig. 7. The reconstructed cross section of the cylinder of example 2 at different generations.

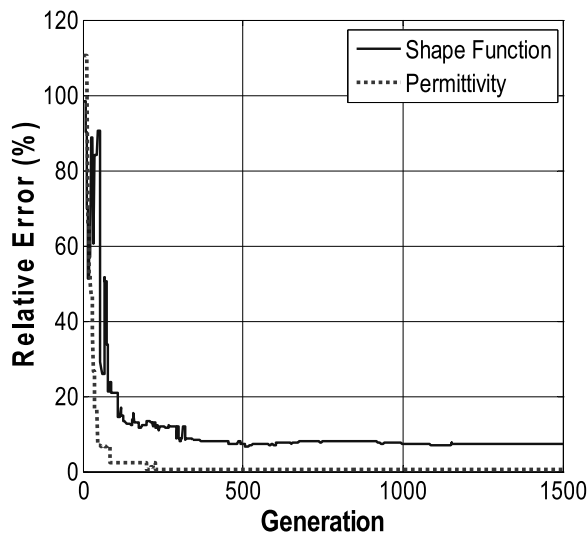


Fig. 8. Shape function error and permittivity error at sequential generations of example 2.

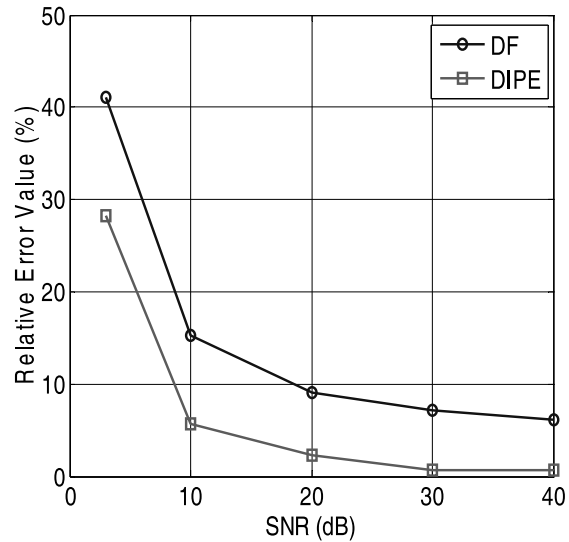


Fig. 9. Shape error as functions of noise for example 2.

that the relative errors of the shape and the permittivity decrease quickly and good convergences are achieved within 500 generations. It also shows the permittivity converges faster than shape function to the corresponding exact values. The r.m.s. error DF is about 7% and DIPE = 0.6% in final generation. From the reconstructed results of this example, we conclude the proposed method is able to reconstruct buried dielectric cylinder successfully when the dielectric object with high-contrast permittivity.

In order to investigate the sensitivity of the imaging algorithm against random noise, the additive white Gaussian noise of zero mean with standard deviation σ_g is added into the scattered electric fields to

mimic the measurement errors. The signal to noise ratio (SNR) is defined as:

$$SNR = 10 \log_{10} \frac{\sum_{n=1}^{N_i} \sum_{m=1}^{M_i} \sum_{b=0}^B |E_z^{\text{exp}}(n, m, b\Delta t)|^2}{\sigma_g^2(N_i)(M_i)(B)} \quad (7)$$

Figure 9 shows the reconstructed results for the cylinder under the condition that the recorded scattered fields are contaminated by noise, of which the SNR includes 40dB, 30dB, 20dB, 10dB and 3dB. It is observed that good reconstruction can be obtained for the shape of the cylinder when the SNR is above 10dB.

5. Conclusion

In this paper, a computational approach to microwave imaging of a buried homogeneous dielectric scatterer with arbitrary cross section in time domain has been presented. Scattering fields are obtained by the FDTD methods. The subgridding scheme is employed to closely describe the shape of the cylinder for the FDTD method. The approach has been formulated as a global nonlinear optimization problem and NU-SSGA has been applied. It has been shown that the location, shape and permittivity of the dielectric object can be successfully reconstructed. In our study, good reconstructed results are obtained even when the initial guess is far from the exact one. Numerical results have been carried out and good reconstruction has been obtained even in the presence of white Gaussian noise in experimental data.

References

- [1] M. Dehmollaian and K. Sarabandi, Refocusing through building walls using synthetic aperture radar, *IEEE Transactions on Geoscience and Remote Sensing* **46** (2008), 1589–1599.
- [2] L.-P. Song, C. Yu and Q.H. Liu, Through-wall imaging (TWI) by radar: 2D tomographic results and analyses, *IEEE Transactions on Geoscience and Remote Sensing* **43**(12) (2005), 2793–2798.
- [3] I. Catapano, L. Crocco and T. Isernia, Improved sampling methods for shape reconstruction of 3-D buried targets, *IEEE Transactions on Geoscience and Remote Sensing* **46**(10) (Oct. 2008), 3265–3273.
- [4] F. Soldovieri, R. Solimene and G. Prisco, A multiarray tomographic approach for through-wall imaging, *IEEE Transactions Geoscience and Remote Sensing* **46**(4) (Apr. 2008), 1192–1199.
- [5] F. Soldovieri, F. Ahmad and R. Solimene, Validation of microwave tomographic inverse scattering approach via through-the-wall experiments in semicontrolled conditions, *IEEE Transactions Geoscience and Remote Sensing* **8**(1) (Jan. 2011), 123–127.
- [6] M. Benedetti, D. Lesselier, M. Lambert and A. Massa, Multiple-shape reconstruction by means of multiregion level sets, *IEEE Transactions Geoscience and Remote Sensing* **48**(5) (May 2010), 2330–2342.
- [7] C.H. Sun, C.C. Chiu, W. Chien and C.L. Li, Application of FDTD and dynamic differential evolution for inverse scattering of a two-dimensional perfectly conducting cylinder in slab medium, *Journal of Electronic Imaging* **19** (Dec 2010), 043016.
- [8] C.H. Sun, C.C. Chiu and C.J. Lin, Image reconstruction of inhomogeneous biaxial dielectric cylinders buried in a slab medium, *International Journal of Applied Electromagnetics and Mechanics* **34**(1, 2) (Nov 2010), pp. 33–48.
- [9] C.H. Sun, C.C. Chiu, C.L. Li and C.H. Huang, Time domain image reconstruction for homogenous dielectric objects by dynamic differential evolution, *Electromagnetics* **30**(4) (May 2010), 309–323.
- [10] M.R. Hajishashem and M.E. Shenawee, Level set algorithm for shape reconstruction of non-overlapping three-dimensional penetrable targets, *IEEE Transactions Geoscience and Remote Sensing* **50**(1) (Jan 2012), 75–86.
- [11] D. Colton and R. Kress, *Inverse Acoustic and Electromagnetic Scattering Theory*, Springer-Verlag, New York, 1992.
- [12] P. Mojabi and J. LoVetri, Overview and classification of some regularization techniques for the gauss-newton inversion method applied to inverse scattering problems, *IEEE Transactions on Antennas and Propagation* **57**(9) (Sept 2009), 2658–2665.

- [13] C.C. Chiu and P.T. Liu, Image reconstruction of a perfectly conducting cylinder by the genetic algorithm, *IEEE Proceeding-Microwaves Antennas and Propagation* **143** (June 1996), 249–253.
- [14] C.H. Sun, C.L. Liu, K.C. Chen, C.C. Chiu, C.L. Li and C.C. Tasi, Electromagnetic transverse electric wave inverse scattering of a partially immersed conductor by steady-state genetic algorithm, *Electromagnetics* **28**(6) (Aug 2008), 389–400.
- [15] W. Chien, C.H. Sun and C.C. Chiu, Image reconstruction for a partially immersed imperfectly conducting cylinder by genetic algorithm, *International Journal of Imaging Systems and Technology* **19** (Dec 2009), 299–305.
- [16] Y.M. Wang and W.C. Chew, An iterative solution of the two-dimensional electromagnetic inverse scattering problem, *International Journal of Imaging Systems and Technology* **1** (1989), 100–108.
- [17] C.C. Chiu, C.H. Sun and Y.S. Fan, Shape reconstruction of 2-D perfectly conducting cylinder targets using the particle swarm optimization, *Imaging Science Journal* **60**(2) (Apr 2012), 83–89.
- [18] W.C. Chew and Y.M. Wang, Reconstruction of two-dimensional permittivity distribution using the distorted born iteration method, *IEEE Trans Med Imag* **9** (Jun 1990), 218–225.
- [19] A. Roger, Newton-Kantorovitch algorithm applied to an electromagnetic inverse problem, *IEEE Transactions on Antennas and Propagation* **29**(Mar 1981), 232–238.
- [20] C.C. Chiu and Y.W. Kiang, Electromagnetic imaging for an imperfectly conducting cylinder, *IEEE Transactions on Microwave Theory and Techniques* **39**(Sept 1991), 1632–1639.
- [21] C.C. Chiu and Y.W. Kiang, Electromagnetic inverse scattering of a conducting cylinder buried in a lossy half-space, *IEEE Transactions on Antennas and Propagation* **40** (Dec 1992), 1562–1565.
- [22] C.L. Li, S.H. Chen, C.M. Yang and C.C. Chiu, Electromagnetic imaging for a partially immersed perfectly conducting cylinder by the genetic algorithm, *Radio Science* **39**(2) (April 2004), RS2016.
- [23] X.-M. Zhong, C. Liao and W. Chen, Image reconstruction of arbitrary cross section conducting cylinder using UWB pulse, *Journal of Electromagnetic Waves Application* **21**(1) (2007), 25–34.
- [24] W. Chien, C.H. Huang, C.C. Chiu and C.L. Li, Image reconstruction for 2D homogeneous dielectric cylinder using FDTD method and SSGA, *International Journal of Applied Electromagnetics and Mechanics* **32**(Feb. 2010), 111–123.
- [25] X. Chen, K. Huang and X.-B. Xu, Microwave imaging of buried inhomogeneous objects using parallel genetic algorithm combined with FDTD method, *Progress in Electromagnetic Research* **PIER 53** (2005), 283–298.
- [26] C.H. Sun, C.L. Li, C.C. Chiu and C.H. Huang, Time domain image reconstruction for a buried 2d homogeneous dielectric cylinder using NU-SSGA, *Research in Nondestructive Evaluation* **22**(1) (Jan. 2011), 1–15.
- [27] M.W. Chevalier, R.J. Luebbers and V.P. Cable, FDTD local grid with material traverse, *IEEE Trans Antennas and Propagation* **45**(3) (March 1997).
- [28] C. de Boor, *A Practical Guide to Splines*, Springer-Verlag, New York, 1978.
- [29] K. Yee, Numerical solutions of initial boundary value problems involving Maxwell's equations in isotropic media, *IEEE Transactions on Antennas and Propagation* **AP-14** (1966), 302–307.
- [30] C.L. Li, C.W. Liu and S.H. Chen, Optimization of a PML Absorber's conductivity profile using FDTD, *Microwave and Optical Technology Letters* **37** (2003), 380–383.
- [31] W. Chien and C.C. Chiu, Using NU-SSGA to reduce the searching time in inverse problem of a buried metallic object, *IEEE Transactions on Antennas and Propagation* **53**(10) (October 2005), 3128–3134.

Copyright of International Journal of Applied Electromagnetics & Mechanics is the property of IOS Press and its content may not be copied or emailed to multiple sites or posted to a listserv without the copyright holder's express written permission. However, users may print, download, or email articles for individual use.